JNC TN8400 99－064

A Study on Pore Structure of Compacted Bentonite (Kunigel-V1)

October, 1999

TOKAI WORKS
JAPAN NUCLEAR CYCLE
DEVELOPMENT INSTITUTE

Ⓣ

圧縮ベントナイト（クニゲルV1）の間隙構造に関する研究

（研究報告）

佐藤治夫*

要　旨

本研究では、拡散に及ぼす圧縮ベントナイトの間隙構造因子の影響を評価するため、非収着性のトリチウム水（HTO）を用いて以下に示す4種類の拡散実験を行った。

(1) 圧縮ベントナイトの圧縮方向をパラメータとした透過拡散実験[圧縮方向の影響]
(2) 圧縮ベントナイト中の珪砂混合率をパラメータとした非定常拡散実験[珪砂混合率の影響]
(3) 圧縮ベントナイトの初期粒径をパラメータとした非定常拡散実験[初期粒径の影響]
(4) 圧縮ベントナイト中に単一亀裂がある場合の含水修復期間をパラメータとした非定常拡散実験[亀裂の影響]

(1)については、クニゲルV1とクニピアF（クニゲルV1を精製してNa型スメクタイトを95wt%以上にしたもの）を対象に、乾燥密度1.0と1.5Mg·m^{-3}に対して実効拡散係数（De）を圧縮方向を変えて測定した。(2)については、クニゲルV1を対象に、見掛けの拡散係数（Da）を乾燥密度0.8, 1.4, 1.8Mg·m^{-3}、珪砂混合率30と50wt%に対して測定した。(3)については、粒径が0.1～5mmと粉末状であるクニゲルV1より大きい、粒状ベントナイト（OT-9607）を対象に、Daを乾燥密度0.8, 1.4, 1.8Mg·m^{-3}に対して測定した。(4)については、乾燥密度1.8Mg·m^{-3}の含水飽和ベントナイトに人工的に貫通した亀裂を入れ、7または28日間再含水させ、Daを測定した。

(1)については、クニゲルV1には全密度ともDeに圧縮方向依存性は見られなかったが、クニピアFでは、圧縮方向に対して直角方向からの方が軸方向からより大きなDeとなった。(2)のベントナイト中の拡散係数に及ぼす珪砂混合率の影響については、全乾燥密度ともDaに影響は見られなかった。(3)の拡散係数に及ぼす初期ベントナイト粒径の影響については、粒状ベントナイト（OT-9607）に対するDaが粉末状であるクニゲルV1の場合と全密度ともほぼ同じであり、ベントナイトの初期粒径の影響は見られなかった。(4)のベントナイト中の単一亀裂の修復特性については、Daに及ぼす亀裂の修復期間依存性や亀裂の影響は見られなかった。

これらのことから、圧縮ベントナイト（クニゲルV1）の間隙構造は、ベントナイトの圧縮方向の影響、珪砂混合率の影響、及び初期粒径の影響を受けにくく、貫通した亀裂が発生した場合においても短期間で亀裂は修復され、間隙構造に影響を及ぼさないと言える。

*核燃料サイクル開発機構　東海事業所　環境保全・研究開発センター
処分研究部　放射化学研究グループ

A Study on Pore Structure of Compacted Bentonite (Kunigel-V1)

Haruo Sato*

Abstract

Four kinds of diffusion experiments; (1) through-diffusion(T-D) experiments for compaction direction dependency, (2) in-diffusion(I-D) experiments for composition dependency of silica sand in bentonite, (3) I-D experiments for initial bentonite grain size dependency, and (4) I-D experiments for the restoration property of an artificial single fracture in compacted bentonite, were carried out using tritiated water which is a non-sorbing nuclide to evaluate the effect of pore structural factors for compacted bentonite on diffudion. For (1), effective diffusivities(De) in Na-bentonites, Kunigel-V1® and Kunipia-F® were measured for 1.0 and 1.5 $Mg \cdot m^{-3}$. For (2), apparent diffusivities(Da) in Kunigel-V1® were measured for 0.8, 1.4 and 1.8 $Mg \cdot m^{-3}$ with silica sand of 30 and 50 wt%. For (3), Da values for 0.8, 1.4 and 1.8 $Mg \cdot m^{-3}$ were measured for a granulated Na-bentonite, OT-9607® which grain-size distribution is in a range between 0.1 and 5 mm. For (4), Da values in Kunigel-V1® which a single fracture was artificially reproduced and was immersed in distilled water for 7 or 28 days for the restoration of the fracture, were measured for 1.8 $Mg \cdot m^{-3}$. Although De values in Kunigel-V1® were approximately the same for both compacted directions over the density, De values for perpendicular direction to compacted direction were higher than those for the same direction as compacted direction in Kunipia-F®. For composition dependency of silica sand in bentonite, no significant effect of the mixure of silica sand in bentonite on Da was found. For initial bentonite grain size dependency, Da values obtained for OT-9607® were approximately the same as those for Kunigel-V1® and no effect of initial grain size of bentonite on diffusion was found. For the restoration property of a single fracture in compacted bentonite, no restoration period dependency on Da was found. Based on this, it may be said that diffusion of nuclides in compacted bentonite, Kunigel-V1® is independent of compaction direction of bentonite, composition of silica sand in bentonite, and initial bentonite grain size. Furthermore, no matter how a penetrated fracture was formed in bentonite, the fracture is restored for a short while.

* Radiochemistry Group, Waste Isolation Research Division,
Waste Management and Fuel Cycle Research Center, Tokai Works,
Japan Nuclear Cycle Development Institute

Contents

Figures

Tables

Appendices

1. INTRODUCTION

In performance assessment of the geological disposal of high-level radioactive waste (HLW), the diffusion of radionuclides in bentonite which composes the multibarrier system, is considered to receive the effect of various pore structural parameters, such as porosity, density, tortuosity, the composition of additives in the bentonite, bentonite grain size, etc. In the multibarrier system of the geological disposal of HLW, since Na-bentonite is considered as a candidate buffer material, the diffusion of radionuclides for Na-bentonite was discussed.

The author and the other researchers have reported bentonite density dependencies for apparent diffusion coefficients (Da) and effective diffusion coefficients (De) of radionuclides in bentonite so far[e.g. 1–6]. The density dependencies simultaneously mean also porosity dependencies, because the porosity is directly related to density. For the effect of the composition of silica sand in bentonite on diffusion, De values of ^{125}I (I^-), ^{36}Cl (Cl^-), ^{14}C (CO_3^{2-}) [7] and HTO[8] in a Na-bentonite, Kunigel-V1® have been reported for a dry density of 1.6 $Mg \cdot m^{-3}$ by Kato et al. The De values showed a tendency to increase with increasing the composition of silica sand in the bentonite, but it was insignificant up to the composition 70 wt%. This indicates there is a possibility that the composition of silica sand in bentonite insignificantly affect pore structural parameters in diffusion. However, the effect of composition of additives in bentonite and bentonite grain size on diffusion has not been systematically studied. Both parameters are possible to affect also tortuosity which expresses the ratio of actually diffused path length to the sample thickness and it is important to understand the diffusion mechanism of radionuclides in bentonite.

In this study, physical factors which are considered to affect the diffusion of radionuclides in bentonite, particularly the effect of pore structural factors for compacted bentonite on diffusion, such as the orientation property of clay particle, the composition of silica sand in bentonite, initial bentonite grain size, and the restoration property of a single fracture in bentonite, were evaluated based on experimental data.

2. EXPERIMENTAL

Four kinds of diffusion experiments; (1) through-diffusion (T-D) experiments for compaction direction dependency, (2) in-diffusion (I-D) experiments for composition dependency of silica sand in bentonite, (3) I-D experiments for initial bentonite grain size dependency, and (4) I-D experiments for the restoration property of a single fracture in compacted bentonite, were carried out using tritiated water (HTO) in order to evaluate the pore structural factors of compacted bentonite on diffusion described above.

2.1 T-D Experiments for Compaction Direction Dependency on De

Effective diffusion coefficients of HTO in Na-bentonites, Kunigel-V1® (composition of Na-smectite, 46–49 wt%) and Kunipia-F® (composition of Na-smectite, over 95 wt%) were measured for the same direction as compacted direction and parpendicular direction to compacted direction for the dry densities of 1.0 and 1.5 $Mg \cdot m^{-3}$ at room temperature by T-D method[9]. The detailed mineralogy for these bentonites is described in the literatures of Ito et al.[10, 11].

Figure 1 shows the sectional view of a diffusion cell for the T-D experiment and the enlargement of the sample holder. The diffusion cell consists of a tracer cell, a measurement cell and a sample holder. The sample holder is set between both cells and bentonite is also filled in this holder. The tracer cell is additionally connected with a tracer tank with a volume of 1 dm^3 to keep the concentration of the tracer in the tracer cell constant and the solution is circulated by a pump.

The bentonite was dried at 105 °C over night and packed into the sample holder of the diffusion cell to obtain the dry densities of 1.0 and 1.5 $Mg \cdot m^{-3}$ with the size of 15x15x15 mm. Ordinarily a disk-typed sample is used, but cubic sample was used in this study, because diffusion direction to compacted direction had to be changed. The bentonite in the holder was saturated with synthetic porewater for 3 days under atmospheric pressure after degassed a half hour in a vacuum chamber.

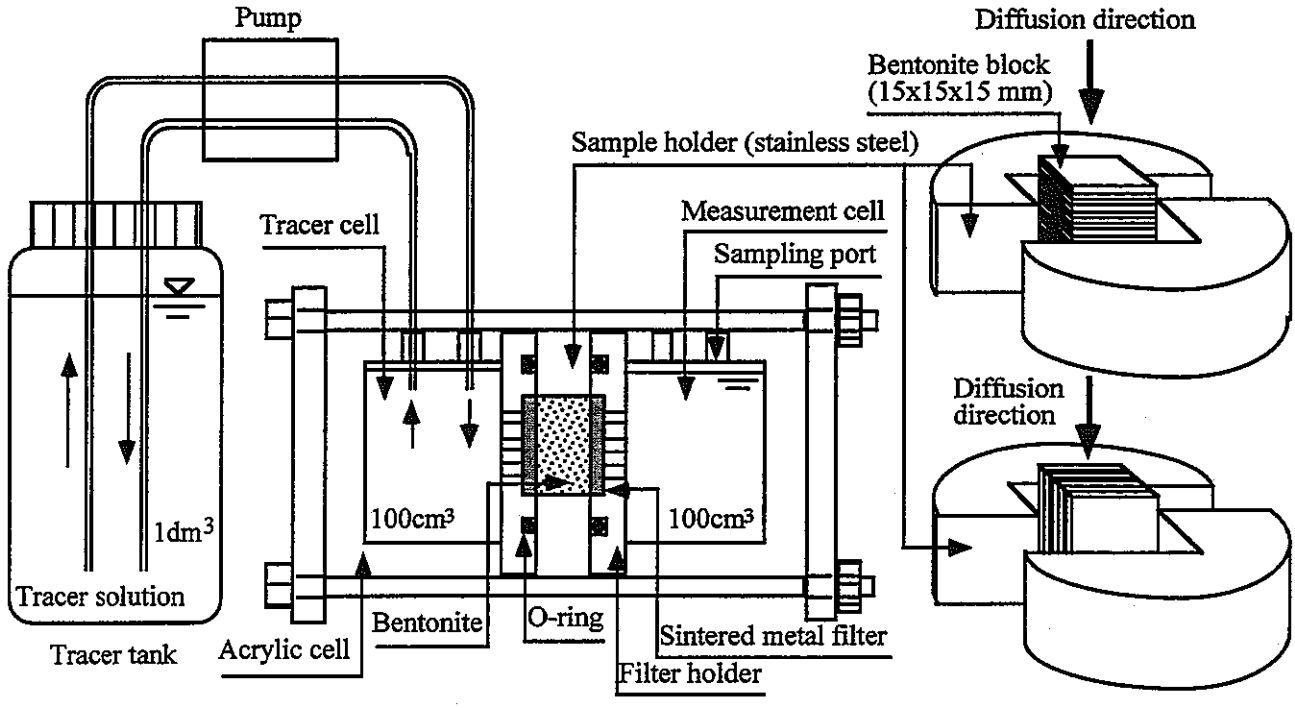

Figure 1 Sectional view of a diffusion cell and the enlargement of the sample holder

Table I Chemical composition of the synthetic porewater

Bentonite	Dry density [$Mg \cdot m^{-3}$]	Na^+[M]	Cl^-[M]	SO_4^{2-}M]	CO_3^{2-}[M]
Kunigel-V1	1.0	0.23	0.002	0.024	0.091
	1.5	0.51	0.0044	0.052	0.20
Kunipia-F	1.0	0.37	0.021	0.0052	0.17
	1.5	0.77	0.045	0.011	0.35

Table I shows the chemical composition of the sythetic porewater. The synthetic porewater was prepared by dissolving NaCl, Na_2CO_3 and Na_2SO_4 in distilled water. The concentration and chemical composition were determined based on the results of bentonite leaching tests for various liquid-solid ratios. After the saturation of the bentonite, the porewater in the tracer cell was exchanged with synthetic porewater added 1.5 kBq•cm^{-3} HTO (90 kcpm•cm^{-3}) and then the experiment was started.

Samples, 0.5 cm^3, were periodically taken from the measurement cell. To minimize the effect of the decrease of the porewater by sampling, when total volume of the porewater decreased up to 95 cm^3, the porewater in the measurement cell was exchanged with synthetic porewater, in which no tracer is contained.

T-D tests for sintered metal filters were also carried out to correct concentration gradients in the filters when De values are calculated. The concentration of HTO was analyzed for 20 minutes with a liquid scintillation counter.

The accumulative quantity of HTO permeated through bentonite from the tracer cell was obtained with time based on those analyzed data. In this study, the accumulative quantity was calculated from the following equation.

$$Qn = Cn \cdot \{V - (n-1) \cdot v\} + \sum_{i=1}^{n-1} (C_i \cdot v) \quad (n = 1, 2, 3, 4, \bullet\bullet\bullet\bullet\bullet) \qquad (1)$$

Where Qn is the accumulative quantity of the tracer permeated through bentonite up to the n-th sampling (cpm), Cn is the analyzed concentration in the n-th sample (cpm•cm^{-3}), V is the solution volume in the measurement cell (cm^3), and v is the sampling volume (cm^3)(0.5 cm^3).

At the end of diffusion experiment, bentonite in the holder was pushed out and cut with a knife into 1 mm pitched slices. Each slice was immediately weighed and dried at 105 °C for over night to obtain water content. The slices were immersed in a 2 cm^3 HCl solution (0.1 M) for over night to extract HTO from the slices. Furthermore, a 18 cm^3 liquid scintillator was added to individual solutions. The concentrations of HTO were then analyzed and the concentration profiles in the bentonite were determined.

2.2 SEM (Scanning Electron Microscope) Observations for the Cross Section of Compacted Bentonite

The SEM observations for the sample cross section to axial and perpendicular directions to compacted direction were carried out for the dry densities of 1.0, 1.6 and 2.0 Mg•m^{-3} to check the clay particle orientation property of the saturated bentonite in compacted state. The observations were carried out for both Kunigel-V1® and Kunipia-F®.

The bentonite was dried at 50 °C for 24 hours to begin with and filled in a column to obtain the dry densities of 1.0, 1.6 and 2.0 Mg•m^{-3} with cylindrical core. The bentonite in the column was saturated with synthetic porewater and frozen in liquid nitrogen after pushed out of the column. The sample was then dried in a vaccum chamber. The cylindrical bentonite was sliced in the axial and perpendicular directions to compacted direction. The SEM observations were carried out for both directions with a magnification of 200 times.

2.3 I-D Experiments for Composition Dependency of Silica Sand in Bentonite on Da

Apparent diffusion coefficients of HTO in Kunigel-V1® were measured for the dry densities of 0.8, 1.4 and 1.8 $Mg \cdot m^{-3}$ with silica sand of 30 and 50 wt% at room temperature by I-D method[e.g. 2]. The bentonite dried at 105 °C over night was filled in the space of a diffusion column together with silica sand to obtain the dry densities of 0.8, 1.4 and 1.8 $Mg \cdot m^{-3}$ with the size of ϕ20x20 mm, and then saturated with distilled water for a week under atmospheric pressure after degassed a half hour in a vacuum chamber. In this case, coarse and fine particle sizes of silica sand (particle size: 1~5 mm and 0.1~1 mm, respectively) was mixed in the bentonite to obtain 30 or 50 wt% with a ratio of 1 to 1 in wt%.

Figure 2 shows the sectional view of a diffusion column. The column is made of stainless steel and a cylindrical space of 20 mm in diameter and 20 mm in thickness is cored inside of the column so that bentonite can be filled in it. A small amount of HTO (25 mm^3: 1.25 kBq) with a concentration of 50 $kBq \cdot cm^{-3}$ was pipetted on the surface of one end of each bentonite and 2 columns were connected at the surface of the bentonite where the tracer was pipetted as shown in **Figure 2** and allowed to diffuse for 1.5 to 8 hours according to density. At the end of all experiments, the cylindrical bentonite was pushed out and cut with a knife into 1mm pitched slices. Each slice was immediately weighed and dried at 105 °C for over 3 hours to obtain water content. The slices were immersed in a 2 cm^3 sodium hexametaphosphate solution for 3 hours shaking to extract HTO from the slices and a liquid scintillator of 18 cm^3 was added. The concentrations of HTO were analyzed with a liquid scintillation counter and the concentration profiles in the bentonite were determined.

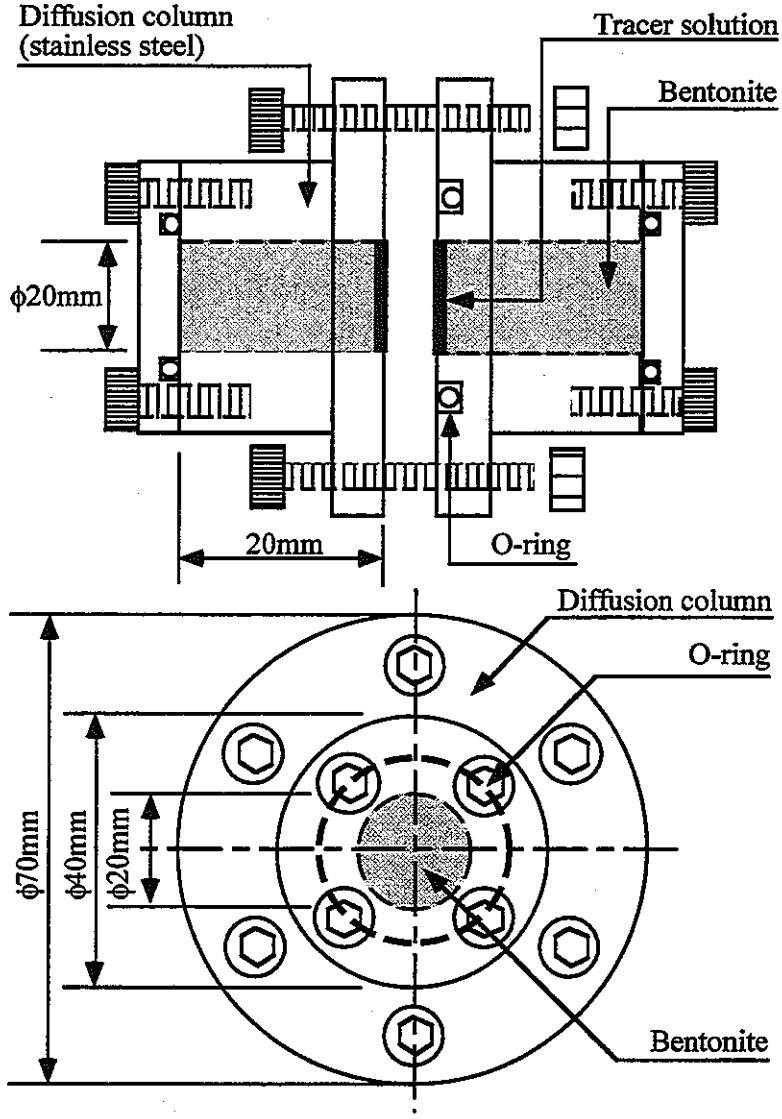

Figure 2 Sectional view of a diffusion column

2.4 I-D Experiments for Initial Bentonite Grain Size Dependency on Da

The Da values of HTO for a granulated Na-bentonite, OT-9607® were measured at room temperature for the dry densities of 0.8, 1.4 and 1.8 $Mg \cdot m^{-3}$. The difference between OT-9607® and Kunigel-V1® is basically only the grain size, and the composition of constituent minerals is approximately the same.

The bentonite with the grain sizes under 2 mm is collected as the OT-9607® and that with the grain sizes under 250 mesh (about 60 μm) is collected as the Kunigel-V1® after crushing. The grain-size distribution of original OT-9607® actually measured is approximately between 0.1 and 5 mm. The detailed fundamental properties such as grain-size distribution and montomorillonite content for OT-9607® are described in the literature of Fujita et al.[12].

All experiments were carried out by I-D method and the experimental procedure was carried out in the same way as that in I-D experiments for composition dependency of silica sand in bentonite. The diffusing period in these experiments was between 2.5 and 7 hours according to density.

2.5 I-D Experiments for the Restoration Property of a Single Fracture in Compacted Bentonite

Compacted bentonite samples (Kunigel-V1®) for a dry density of 1.8 $Mg \cdot m^{-3}$ were prepared, and then saturated with distilled water in the same way as that in I-D experiments for composition dependency of silica sand in bentonite. After the saturation, a single fracture was artificially reproduced by inserting an acrylic spacer with a thickness of 1 mm, and then the bentonite samples with fracture were immersed in distilled water for 7 or 28 days again for the restoration of the fracture. **Figure 3** shows an image of the bentonite with an artificial single fracture.

After the resaturation for 7 or 28 days, Da values of HTO were measured for these bentonite

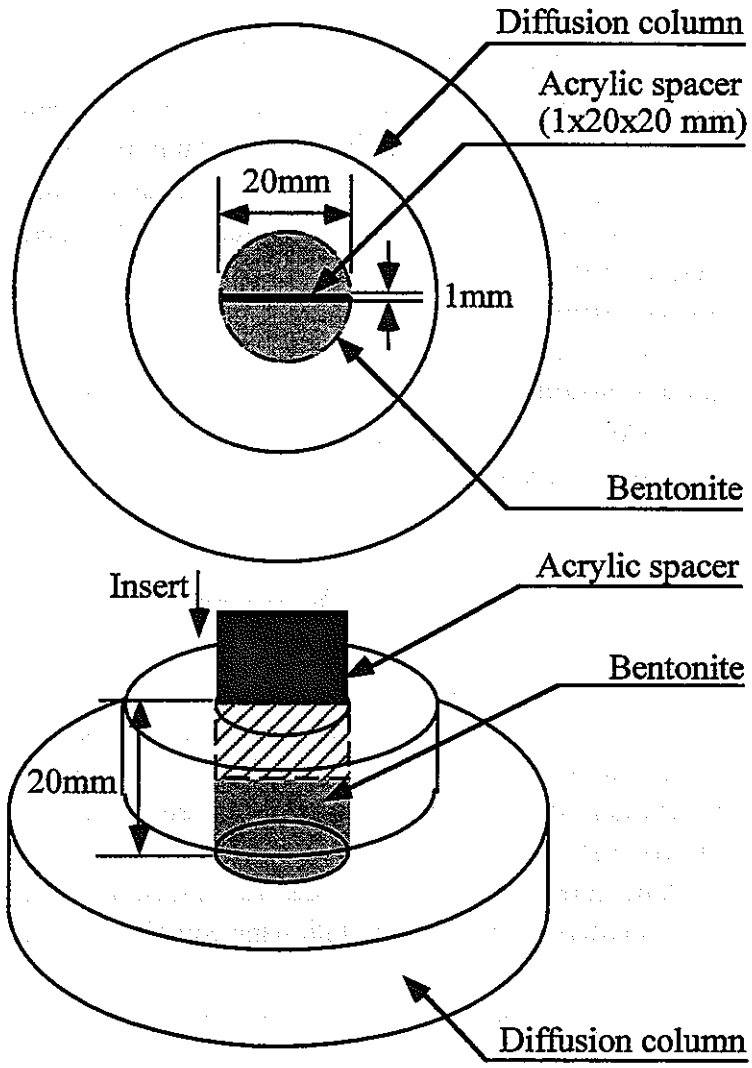

Figure 3 An image of bentonite with an artificial single fracture

samples by I-D method. No fracture was apparently observed on the surface of bentonite specimen after the resaturation for 7 or 28 days. The experimental procedure and the amount of tracer (HTO) pipetted on the surface of the bentonite were carried out in the same way as those described above. The diffusing period in these experiments was 7 hours.

3. DIFFUSION THEORY AND ANALYTICAL METHODS

3.1 Calculation of De

The calculations of De and Da values were based on Fickian law[13]. The diffusion equation for a one-dimensional non-steady state is generally expressed by the following equation[14].

$$\frac{\partial C}{\partial t} = \left(\frac{\phi \cdot Dp}{\alpha}\right) \cdot \frac{\partial^2 C}{\partial x^2} \qquad (2)$$

Where C is the concentration of the tracer in the bentonite ($kg \cdot m^{-3}$), t is the diffusing time (s), Dp is the diffusion coefficient in the porewater ($m^2 \cdot s^{-1}$), ϕ is the porosity, α is the rock capacity factor ($\alpha = \phi + \rho \cdot Kd$), ρ is the dry density of the sample ($Mg \cdot m^{-3}$), Kd is the distribution coefficient ($m^3 \cdot Mg^{-1}$), and x is the distance from the source (m).

The $\phi \cdot Dp/\alpha$ is equal to Da. The accumulative quantity of the tracer permeated through bentonite up to an arbitrary time for equation (2), based on initial and boundary conditions, is written as follows:

Initial condition

$C(t, x) = 0, t = 0, 0 \leq x \leq L$

Boundary condition

$C(t, x) = Co \cdot \alpha, t > 0, x = 0$

$C(t, x) = 0, t > 0, x = L$

$$Q(t) = A \cdot L \cdot Co \cdot \left[\frac{De}{L^2}t - \frac{\alpha}{6} - \frac{2\alpha}{\pi^2}\sum_{n=1}^{\infty}\left\{\frac{(-1)^n}{n^2}\exp\left(\frac{De \cdot n^2 \cdot \pi^2 \cdot t}{L^2 \cdot \alpha}\right)\right\}\right] \qquad (3)$$

Where Q(t) is the accumulative quantity of the tracer permeated through bentonite (cpm), A is the cross-section area of the sample (m^3), L is the thickness of the sample (m), Co is the concentration of the tracer in the tracer cell ($cpm \cdot cm^{-3}$), and De is the effective diffusion coefficient ($m^2 \cdot s^{-1}$).

At long time such as steady state, the exponentials fall away to zero. Therefore, equation (3) is approximately written by the following equation for steady state.

$$Q(t) = A \cdot L \cdot Co \cdot \left(\frac{De}{L^2}t - \frac{\alpha}{6}\right) \qquad (4)$$

The De is calculated from the slope of Q(t) with time in steady state based on equation (4).

If surface diffusion does not occur, De is expressed by the following parameters[14, 15].

$$De = \phi \cdot \left(\frac{\delta}{\tau^2} \right) \cdot Do = \phi \cdot G \cdot Do = FF \cdot Do \quad (5)$$

Where δ is the constrictivity (–), τ^2 is the tortuosity (–), Do is the free water diffusion coefficient ($m^2 \cdot s^{-1}$), G is the geometric factor(or tortuosity factor), and FF is the formation factor (–).

It is familiar that Do depends on species. The Do is calculated by the Nernst expression[16] as shown below.

$$Do = \frac{R \cdot T \cdot \lambda}{F^2 \cdot Z} \quad (6)$$

Where R is the gas constant (8.314 $J \cdot mol^{-1} \cdot K^{-1}$), T is the absolute temperature (K), λ is the limiting ionic equivalent conductivity ($m^2 \cdot S \cdot mol^{-1}$), F is the Faraday constant (96,493 $C \cdot mol^{-1}$), and Z is the absolute value of the ionic charge.

Tritiated water, part of water molecule was exchanged with ^3H, can be regarded as a neutral species. Therefore, since Do can not be obtained by electrical measurement, Do directly measured by a diffusion experiment is reported. In this case, since water diffuses in the water, Do is called a self-diffusion coefficient and is reported to be 2.28×10^{-9} $m^2 \cdot s^{-1}$ (25°C) for HTO[17].

The concentration gradient of tracer in the filter which was used to constrict the swelling of bentonite is also included in De calculated based on equation (4) and this concentration gradient in the filter must be corrected to calculate true De in bentonite. In this study, De was corrected by the following equation derived for steady state[18].

$$De = \frac{L}{\left(\frac{L + 2L_f}{De_t} \right) - \left(\frac{2L_f}{De_f} \right)} \quad (7)$$

Where Det is the effective diffusion coefficient before correction ($m^2 \cdot s^{-1}$), Def is the effective diffusion coefficient in the filter ($m^2 \cdot s^{-1}$), and Lf is the thickness of the filter (m)(1 mm in this study).

3.2 Calculation of Da

Although De described above is the diffusion coefficient for steady state, Da is one for non-steady state and concentration profile gradually changes with time. Basic equation for a one-dimensional non-steady state diffusion is as given by equation (2). For HTO, since solubility does not exist, analytical solution in case of an instantaneous planar source can be applied for the calculation of Da.

For one-dimensional diffusion of a planar source consisting of a limited amount of substance in a cylinder of infinite length, when it is assumed that the diffusion is independent of the

position, the analytical solution for equation (2) is derived as the following equation[13].

Initial condition

$C(t, x) = 0, t = 0, x \neq 0$

Boundary condition

$C(t, x) = 0, t > 0, x = \pm\infty$

$$M = \int_{-\infty}^{\infty} C\, dx$$

$$C = \frac{M}{2\sqrt{\pi Da \cdot t}} exp\left(-\frac{x^2}{4Da \cdot t}\right) \quad (8)$$

Where M is the total amount of the tracer per unit area ($dpm \cdot m^{-2}$) and Da is the apparent diffusion coefficient ($m^2 \cdot s^{-1}$).

The slope given by a plot of LnC versus x^2 gives Da from the relation of diffusing time based on equation (8). Apparent diffusion coefficient of HTO was determined based on this method.

4. RESULTS AND DISCUSSION

4.1 Compaction Direction Dependency on De and SEM Observations

The concentrations of HTO in the measurement cell as a function of time showed non-linear curves in transient state and increased in a straight line as a function of time in steady state. The concentration profiles of HTO in bentonite approximately linearly decreased from the tracer cell side to the other side in all cases. This indicates that the diffusion in all cases was in steady state.

Figure 4 shows De values of HTO as a function of the dry density of bentonite for compaction direction dependency. **Table II** shows obtained Def and De values. The obtained De values decreased with increasing the dry density of bentonite, showing similar tendency to data reported

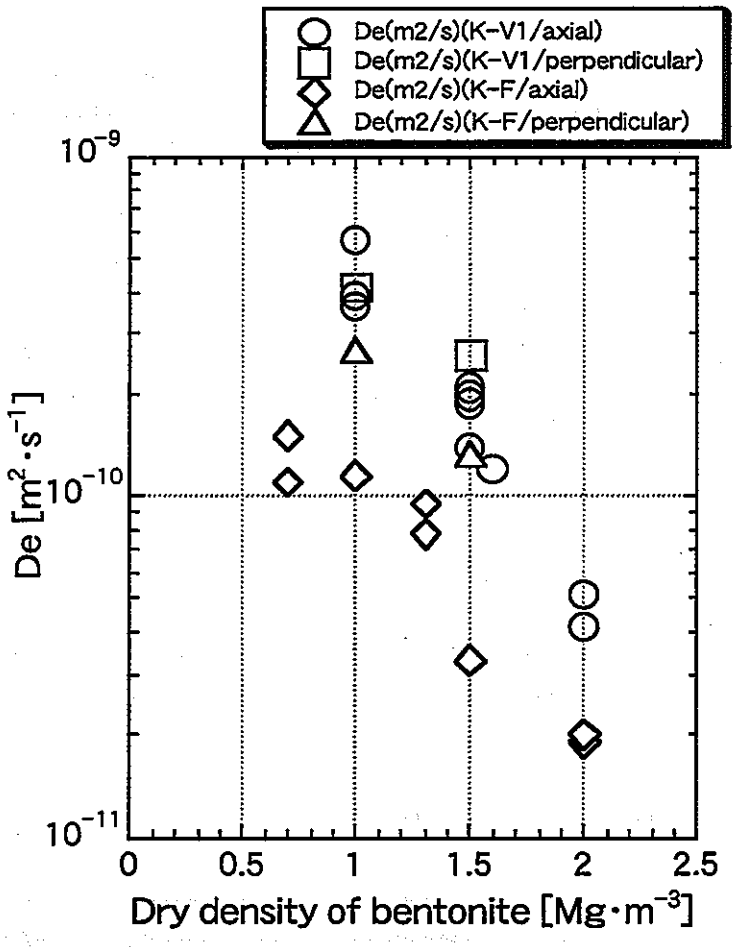

Figure 4 De values of HTO as a function of dry density for compaction direction dependency in diffusion
K–V1: Kunigel-V1®, K–F: Kunipia-F®

to date[5, 19]. Although De values in Kunigel-V1® were approximately the same for both diffusion directions over the density, De values for perpendicular direction to compacted direction were higher than those for the same direction as compacted direction in Kunipia-F®, being approximately 4 times greater than those for a dry density of 1.5 $Mg \cdot m^{-3}$. Although significant dependency for compaction direction on De values in Kunigel-V1® was not found, it seems that De values for perpendicular direction to compacted direction gradually show a tendency to be greater than those for axial direction to compacted direction with increasing bentonite density.

Table II Def and De values obtained for bentonite (Kunigel-V1 and Kunipia-F)

Bentonite	Dry density [$Mg \cdot m^{-3}$]	Diffusion direction	Effective diffusion coefficient [$m^2 \cdot s^{-1}$]	
			Def	De
Kunigel-V1	1.0	axial	2.7E–10	3.9E–10
		perpendicular	2.8E–10	4.1E–10
	1.5	axial	2.1E–10	2.1E–10
		perpendicular	2.1E–10	2.0E–10
Kunipia-F	1.0	axial	3.0E–10	1.2E–10
		perpendicular	3.1E–10	2.7E–10
	1.5	axial	3.0E–10	3.3E–11
		perpendicular	2.5E–10	1.3E–10

Def : effective diffusion coefficient in the filter
De : effective diffusion coefficient in bentonite
axial : diffusion in the same direction as compacted direction (see below)
perpendicular : diffusion in perpendicular direction to compacted direction (see below)

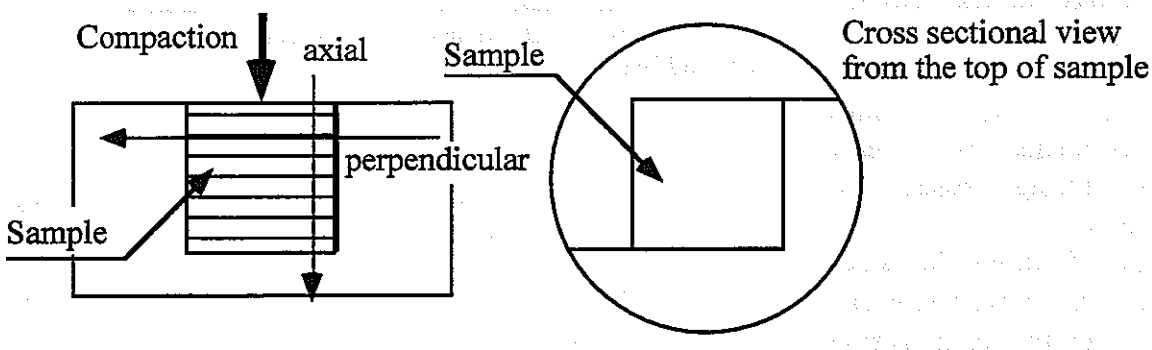

The results of SEM observations showed that no orientation of clay particle was found for Kunigel-V1® over the density(see **Appendix I**: cross-sectional photographs of compacted bentonite (Kunigel-V1® and Kunipia-F®) for the dry densities of 1.0, 1.6 and 2.0 $Mg \cdot m^{-3}$). On the other hand, that was found for Kunipia-F® and the degree of the orientation of clay particle became significant with increasing the bentonite density. This supports the results for

compaction direction dependency in De. Based on this, it is presumed that the composition of smectite in bentonite affects the clay particle orientation property of the bentonite and finally affects also diffusion. Additionally it is predicted that the more significant the degree of orientation becomes, the more significant compaction direction dependency on diffusion becomes.

4.2 Composition Dependency of Silica Sand in Bentonite on Da

The concentrations of HTO decreased with increasing distance squared from the surface of bentonite where tracer (HTO) was pipetted (see **Appendix II**: correlations between concentrations of HTO in bentonite and distance squared from the surface of the bentonite where tracer (HTO) was pipetted). Where the concentration of HTO is shown in dpm•cm^{-3}. Although the actual concentration of HTO per unit volume of bentonite can be calculated from bentonite slice volume, solution volume (20 cm^3) used for removal from the slice and the analyzed concentration of HTO, it is here shown in relative concentration. The Da values were determined by a least squares fitting based on equation (8).

Figure 5 shows Da values as a function of bentonite dry density and the composition of silica sand added in the bentonite. **Table III** shows the obtained Da values of HTO. The plots simultaneously show also Da data obtained in the system without silica sand

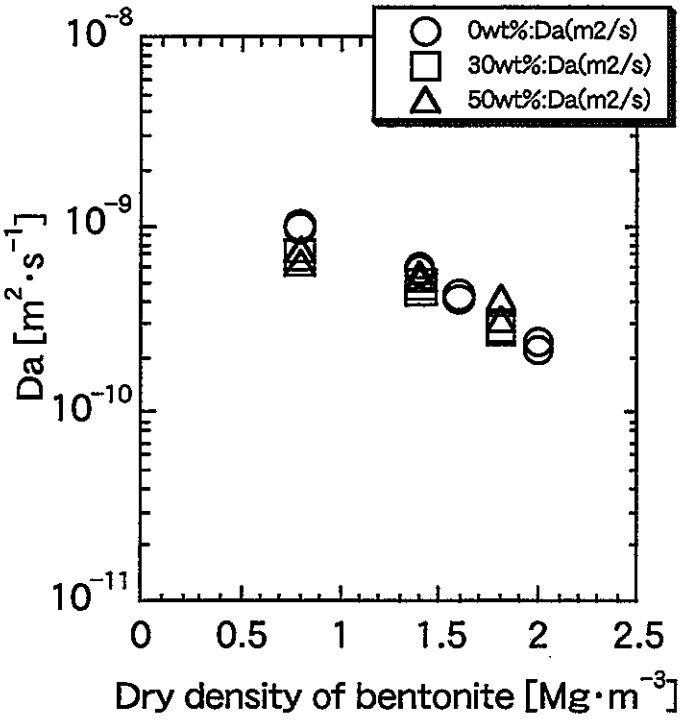

Figure 5 Da values as a function of bentonite dry density and the composition of silica sand added in the bentonite

Table III Da values of HTO obtained for the composition of silica sand in bentonite (Kunigel-V1)

Composition of silica sand [wt%]	Dry density [Mg·m^{-3}]	Diffusing time [h]	Da [m^2·s^{-1}]
30	0.8	1.5	7.1E–10
			7.1E–10
	1.4	4.0	4.5E–10
			4.8E–10
	1.8	7.0	2.9E–10
			2.8E–10
50	0.8	1.5	7.6E–10
			6.3E–10
	1.4	2.5	5.5E–10
			5.2E–10
	1.8	5.0	4.2E–10
			3.2E–10

to compare[5]. As is clear in **Figure 5**, no significant effect of the composition of silica sand in bentonite on Da was found between 0 and 50 wt% at least for Kunigel-V1®. This tendency is consistent with also that for De values of HTO as a function of the composition of silica sand in Kunigel-V1® for a dry density of 1.6 $Mg \cdot m^{-3}$[8].

4.3 Initial Bentonite Grain Size Dependency on Da

The concentrations of HTO in bentonite linearly decreased with increasing distance squared from the surface of the bentonite where tracer (HTO) was pipetted similarly to the results of composition dependency of silica sand in bentonite(see **Appendix III**: correlations between concentrations of HTO in granulated bentonite (OT-9607®) and distance squared from the surface of the bentonite where tracer (HTO) was pipetted). Also where the concentration of HTO is shown in $dpm \cdot cm^{-3}$ similarly to 4.2. All Da values were also determined by a least squares fitting based on equation (8) in the same way as that for the composition dependency of silica sand in bentonite.

Figure 6 shows Da values as a function of the dry density of granulated bentonite, OT-9607. The plots show also Da values obtained for Kunigel-V1® to compare[5]. **Table IV** shows Da values obtained for the granulated bentonite (OT-9607®). The Da values decreased with increasing the dry density of the granulated bentonite similarly to tendency reported to date. Moreover, the obtained Da values were approximately the same as those for initially powder bentonite (Kunigel-V1®)[5] and no effect of initial grain size of bentonite on

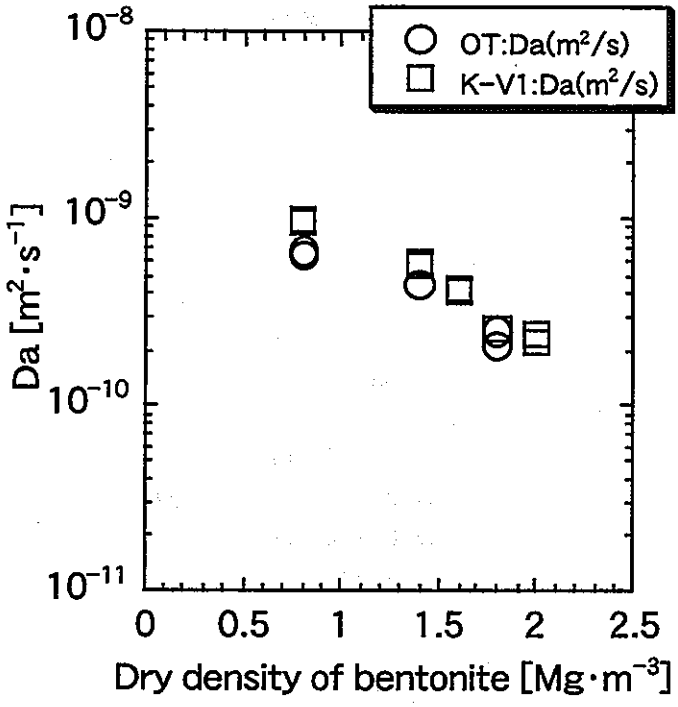

Figure 6 Da values as a function of the dry density of granulated bentonite (OT-9607) and powder bentonite (Kunigel-V1)
OT: OT-9607, K-V1: Kunigel-V1

Table IV Da values of HTO obtained for granulated bentonite (OT-9607)

Dry density [$Mg \cdot m^{-3}$]	Diffusing time [h]	Da [$m^2 \cdot s^{-1}$]
0.8	2.5	6.4E−10
		6.6E−10
1.4	5.0	4.4E−10
		4.4E−10
1.8	7.0	2.5E−10
		2.1E−10

diffusion was found.

4.4 Restoration Property of a Single Fracture in Compacted Bentonite

The concentrations of HTO in bentonite linearly decreased with increasing distance squared from the surface of the bentonite where tracer (HTO) was pipetted (see **Appendix IV**: correlations between concentrations of HTO in bentonite and distance squared from the surface of the bentonite where tracer (HTO) was pipetted). Also where the concentration of HTO is shown in dpm•cm^{-3} similarly to 4.2 and 4.3. The Da values were determined by a least squares fitting based on equation (8).

Figure 7 shows Da values as a function of the dry density of bentonite and resaturation period by distilled water. **Table V** shows Da values as a function of restoration period for compacted bentonite, Kunigel-V1®, in which a single fracture was artificially reproduced. All obtained Da values, independent of fracture and restoration period, were approximately the same. This is presumed because the fracture was sealed by the

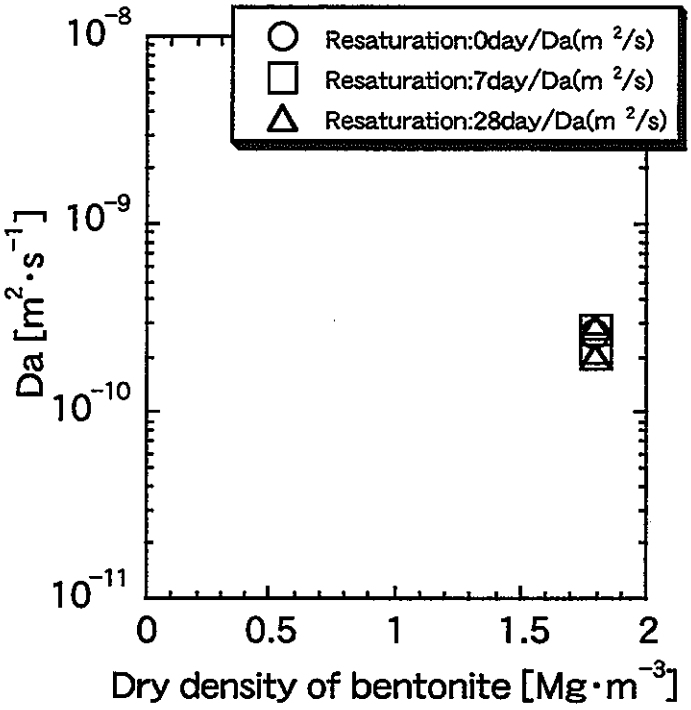

Figure 7 Da values as a function of the dry density of bentonite and the restoration period of artificially reproduced fracture for a dry density of 1.8 Mg•m^{-3}

Table V Da values of HTO as a function of the restoration period of a single fracture in compacted bentonite (Kunigel-V1)

Bentonite condition (with/without fracture)	Restoration (resaturation) period [day]	Da [m^2·s^{-1}]
with fracture	7	2.2E–10 2.7E–10
	28	2.0E–10 2.9E–10
without fracture	——	2.6E–10 2.6E–10

*All experiments were carried out for a dry density of 1.8 Mg•m^{-3}.
**The experiments for bentonite without fracture are the same as normal I–D tests.

swelling of bentonite for a short while. Based on this, it is presumed that no matter how a penetrated fracture was developed in bentonite, the fracture is restored in a short while and it does not affect diffusion.

5. CONCLUSIONS

(1) The composition of smectite in bentonite affects the orientation property of clay particle in the bentonite and finally also affects diffusion. Namely the higher the composition of smectite in bentonite becomes, the more significant the degree of orientation becomes and the degree of compaction direction dependency on diffusion also becomes significant. To the contrary, the composition of silica sand in bentonite and initial bentonite grain size insignificantly affect diffusion.

(2) No matter how a penetrated fracture was formed in bentonite, the fracture is restored in a short while and it does not affect diffusion. Namely the fracture developed in bentonite is sealed for a short while by the swelling of the bentonite.

6. ACKNOWLEDGMENTS

The author would like to thank Messrs. S. Ueta and H. Kato of Mitsubishi Materials Corporation for the performance of the diffusion experiments using HTO.

REFERENCES

1. H. Sato, T. Ashida, Y. Kohara, M. Yui, and N. Sasaki, Effect of Dry Density on Diffusion of Some Radionuclides in Compacted Sodium Bentonite, J. Nucl. Sci. Tech., **29** (9), 873–882 (1992).
2. H. Sato, T. Ashida, Y. Kohara, and M. Yui, Study on Retardation Mechanism of ^{3}H, ^{99}Tc, ^{137}Cs, ^{237}Np and ^{241}Am in Compacted Sodium Bentonite, in *Scientific Basis for Nuclear Waste Management XVI*, edited by C. G. Interrante and R. T. Pabalan (Mater. Res. Soc. Proc. **294**, Pittsburgh, PA, 1993) pp.403–408.
3. H. Sato and M. Yui, Diffusion Behaviour for Se and Zr in Sodium Bentonite, in *Scientific Basis for Nuclear Waste Management XVIII*, edited by T. Murakami and R. C. Ewing (Mater. Res. Soc. Proc. **353**, Pittsburgh, PA, 1995) pp.269–276.
4. H. Sato and M. Yui, Diffusion of Ni in Compacted Sodium Bentonite, J. Nucl. Sci. Tech., **34** (3), 334–336 (1997).
5. H. Sato and T. Shibutani, Study on Adsorption and Diffusion Mechanism of Nuclides in Buffer Material and Geosphere, PNC Technical Review, No.91, PNC TN8410 94-284, 71–89, 1994 (in Japanese).
6. H. Kato, M. Muroi, N. Yamada, H. Ishida, and H. Sato, Estimation of Effective Diffusivity in Compacted Bentonite, in *Scientific Basis for Nuclear Waste Management XVIII*, edited by T. Murakami and R. C. Ewing (Mater. Res. Soc. Proc. **353**, Pittsburgh, PA, 1995) pp.277–284.
7. H. Kato, T. Nakazawa, S. Ueta, M. Muroi, I. Yasutomi, and H. Fujihara, Effective Diffusivities of Iodine, Chlorine, and Carbon in Bentonite Buffer Material, in *Scientific Basis for Nuclear Waste Management XXII*, edited by D. J. Wronkiewicz and J. H. Lee (Mater. Res.

Soc. Proc. **556**, Warrendale, PA, 1999) pp.687–694.
8. H. Kato and T. Yato, Estimation of the Effective Diffusivity in Sand/Bentonite Mixture, 1997 Fall Meeting of the Atomic Energy Society of Japan, I39, p.681 (1997)(in Japanese).
9. A. Muurinen, P. Pentilä-Hiltunen, and J. Rantanen, Diffusion Mechanisms of Strontium and Cesium in Compacted Sodium Bentonite, in *Scientific Basis for Nuclear Waste Management X*, edited by J. K. Bates and W. B. Seefeldt (Mater. Res. Soc. Proc. **84**, Pittsburgh, PA, 1987) pp.803–811.
10. H. Ito, M. Okamoto, M. Shibata, Y. Sasaki, T. Tanbara, K. Suzuki, and T. Watanabe, Mineral Composition Analysis of Bentonite, PNC TN8430 93-003, 1993 (in Japanese).
11. M. Ito, K. Suzuki, M. Shibata, and Y. Sasaki, Mineral Composition Analysis of Bentonite, J. Atomic Energy Soc. Japan, **36** (11), 1055–1058 (1994)(in Japanese).
12. T. Fujita, M. Chijimatsu, H. Ishikawa, H. Suzuki, and K. Matsumoto, Fundamental Properties of Bentonite OT-9607, PNC TN8410 97-071, 1997.
13. J. Crank, *The Mathematics of Diffusion*, 2nd ed. (Pergamon Press, Oxford, 1975).
14. K. Skagius and I. Neretnieks, Diffusion in Crystalline Rocks of Some Sorbing and Nonsorbing Species, KBS TR82-12, 1982.
15. H. Sato, T. Shibutani, and M. Yui, Experimental and Modelling Studies on Diffusion of Cs, Ni and Sm in Granodiorite, Basalt and Mudstone, J. Contaminant Hydrology **26**, 119–133 (1997).
16. R. A. Robinson and R. H. Stokes, *Electrolyte Solutions*, 2nd ed. (Butterworths, London, 1959). p.317.
17. Chemical Society of Japan, *Chemical Handbook*, 4th ed. (Maruzen, Tokyo, 1993). p.II-61 (in Japanese).
18. H. Sato, Effect of Ionic Charge on Effective Diffusion Coefficient in Compacted Sodium Bentonite, in Scientific Basis for Nuclear Waste Management XXIII (Mater. Res. Soc. Proc., XXX, in press).
19. PNC, Annual Report -FY1989-, PNC TN1410 91-009, 51–52, 1991 (in Japanese).

Appendix I-a

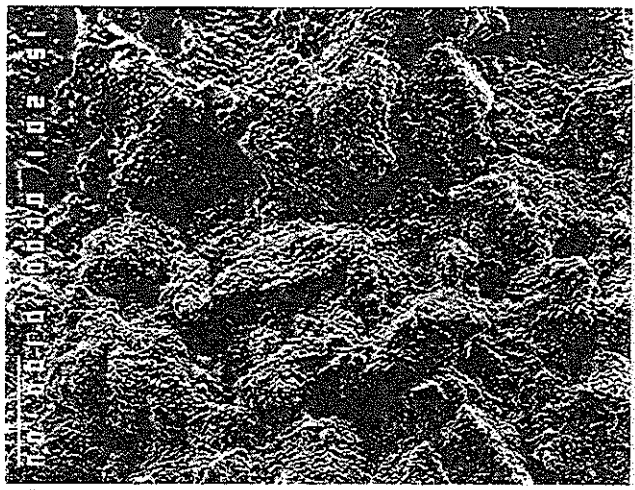

Photograph (a)

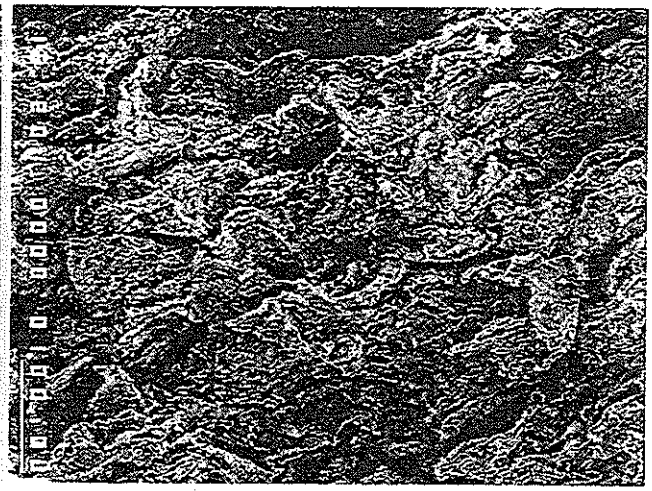

Photograph (c)

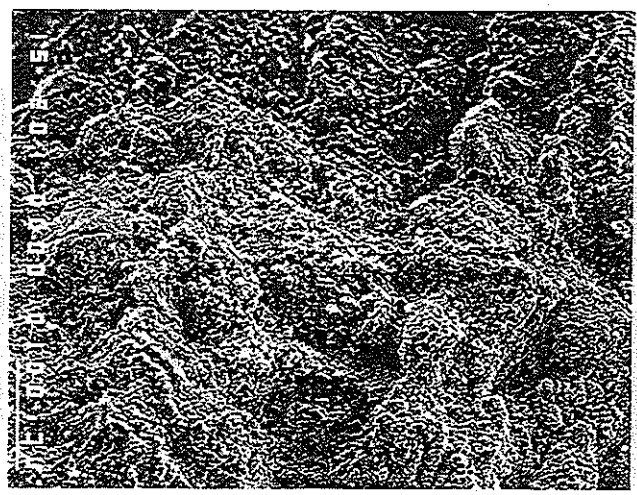

Photograph (b)

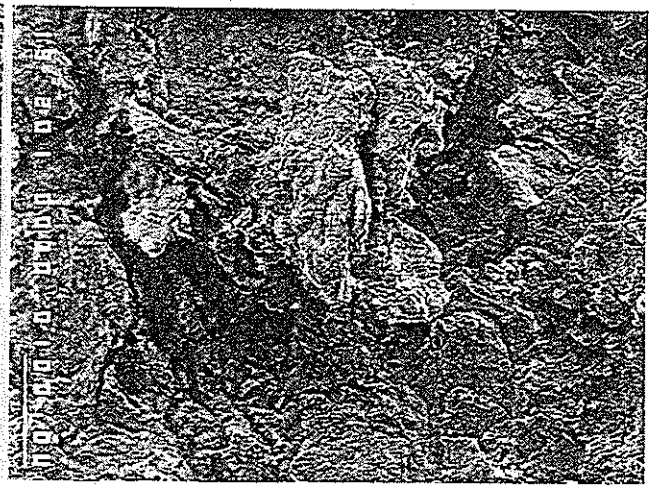

Photograph (d)

Cross-sectional photographs of compacted bentonite for a dry density of 1.0 $Mg \cdot m^{-3}$ (Kunigel-V1 and Kunipia-F) by SEM

(a) cross-sectional photograph for perpendicular direction to compacted direction for Kunigel-V1, (b) cross-sectional photograph for axial direction to compacted direction for Kunigel-V1, (c) cross-sectional photograph for perpendicular direction to compacted direction for Kunipia-F, and (d) cross-sectional photograph for axial direction to compacted direction for Kunipia-F.

Appendix I-b

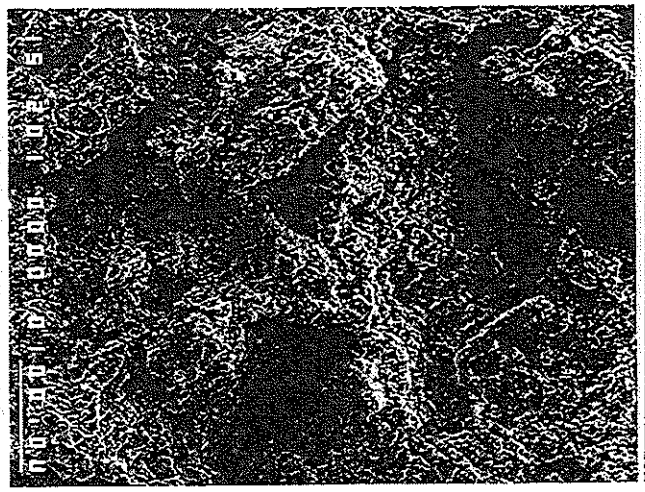

Photograph (a)

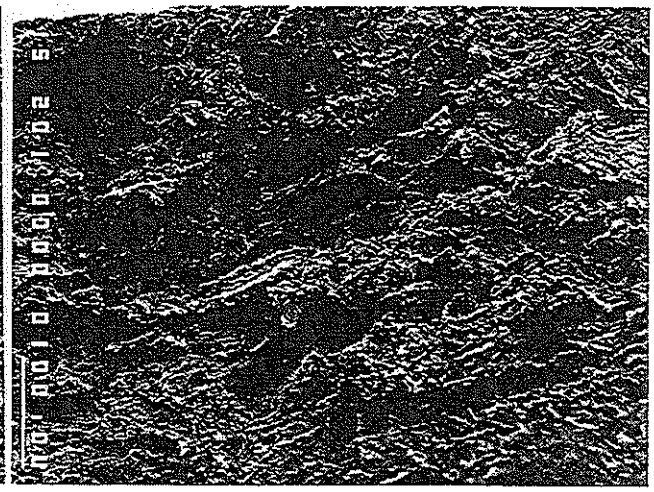

Photograph (c)

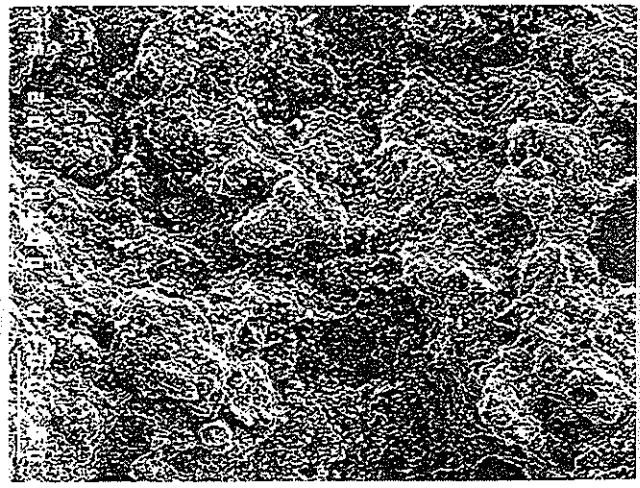

Photograph (b)

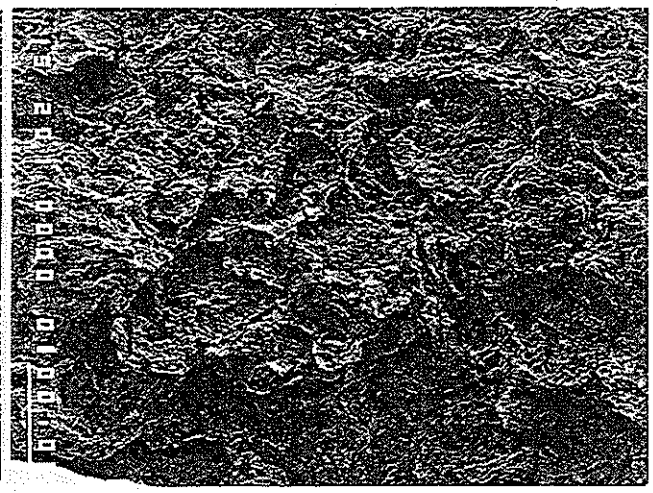

Photograph (d)

Cross-sectional photographs of compacted bentonite for a dry density of 1.6 $Mg \cdot m^{-3}$ (Kunigel-V1 and Kunipia-F) by SEM

(a) cross-sectional photograph for perpendicular direction to compacted direction for Kunigel-V1, (b) cross-sectional photograph for axial direction to compacted direction for Kunigel-V1, (c) cross-sectional photograph for perpendicular direction to compacted direction for Kunipia-F, and (d) cross-sectional photograph for axial direction to compacted direction for Kunipia-F.

Appendix I-c

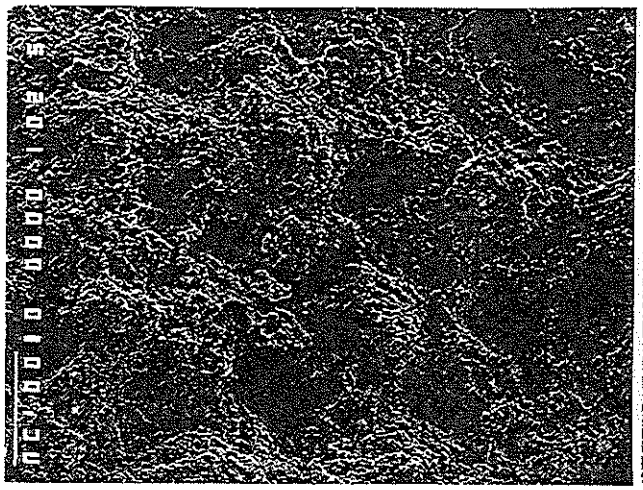

Photograph (a)

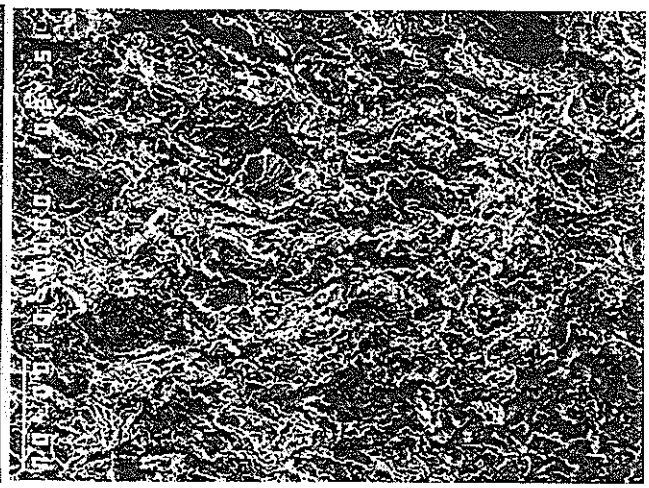

Photograph (c)

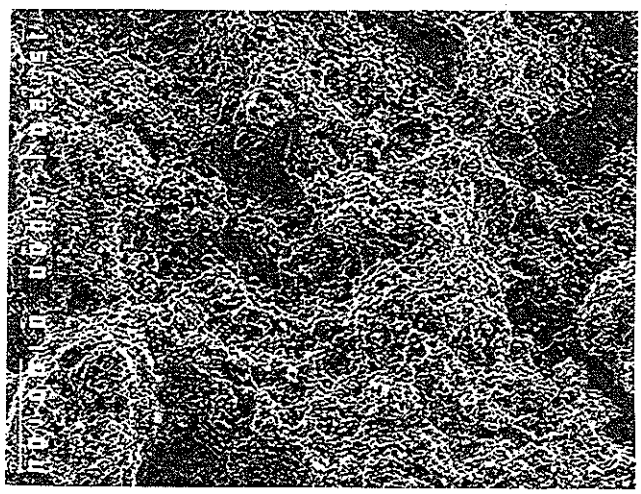

Photograph (b)

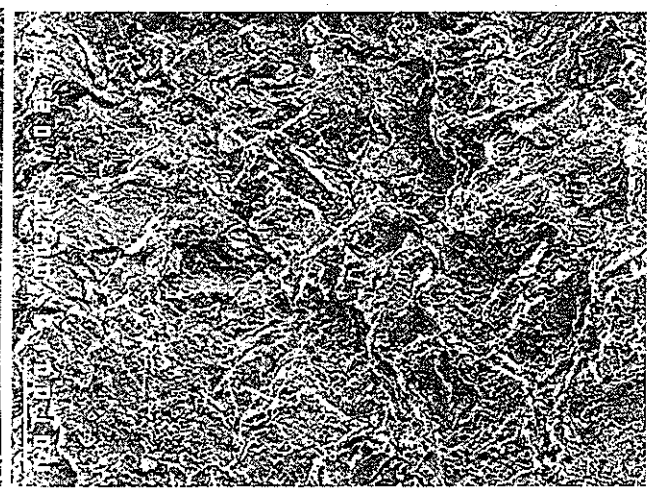

Photograph (d)

Cross-sectional photographs of compacted bentonite for a dry density of 2.0 $Mg \cdot m^{-3}$ (Kunigel-V1 and Kunipia-F) by SEM

(a) cross-sectional photograph for perpendicular direction to compacted direction for Kunigel-V1, (b) cross-sectional photograph for axial direction to compacted direction for Kunigel-V1, (c) cross-sectional photograph for perpendicular direction to compacted direction for Kunipia-F, and (d) cross-sectional photograph for axial direction to compacted direction for Kunipia-F.

Appendix II-a

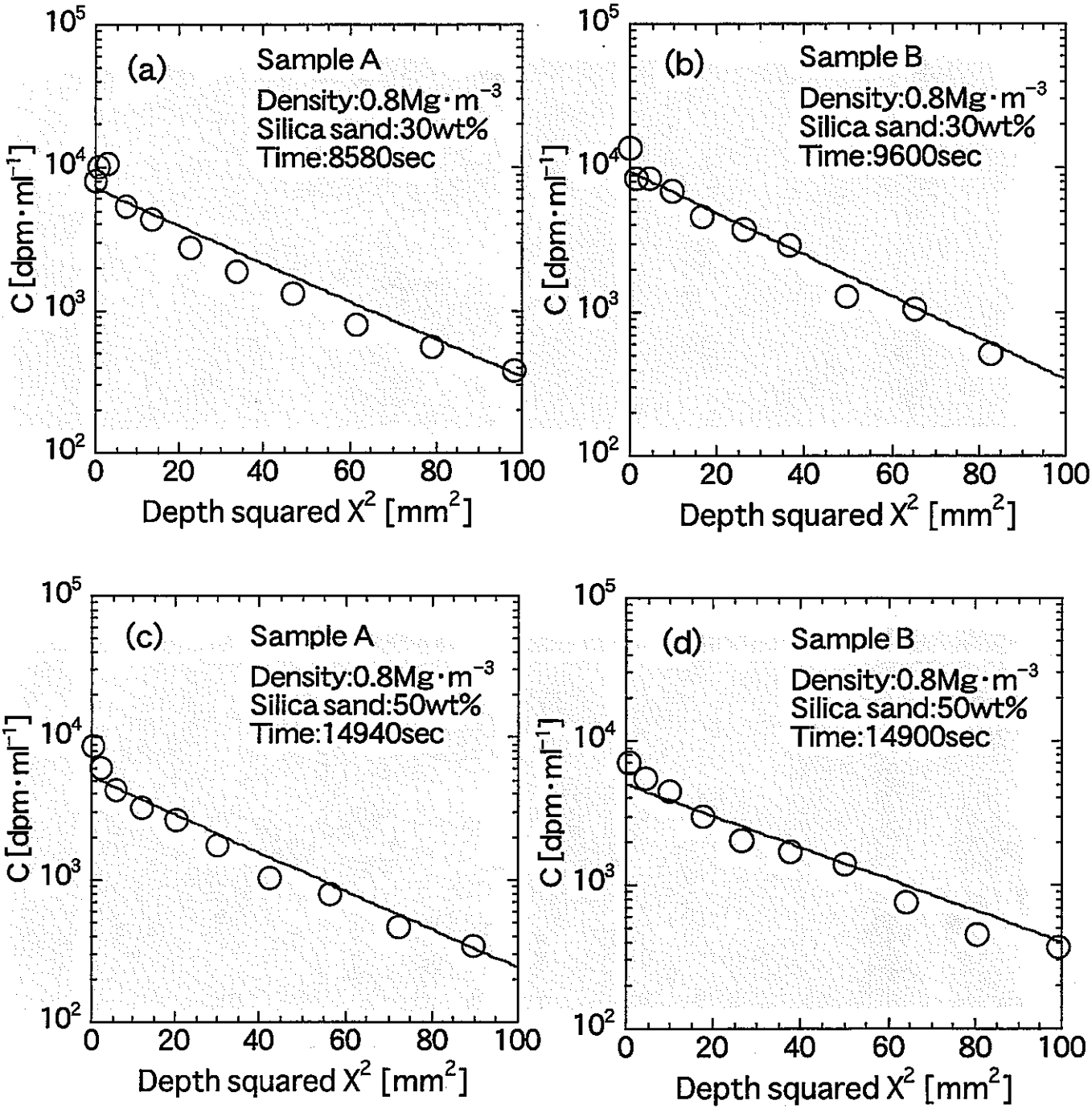

Correlations between the concentrations of HTO in bentonite and depth squared from the surface of the bentonite where tracer was pipetted for a dry density of 0.8 Mg•m^{-3}

(a) and (b); composition of silica sand in the bentonite, 30 wt%

(c) and (d); composition of silica sand in the bentonite, 50 wt%

Appendix II-b

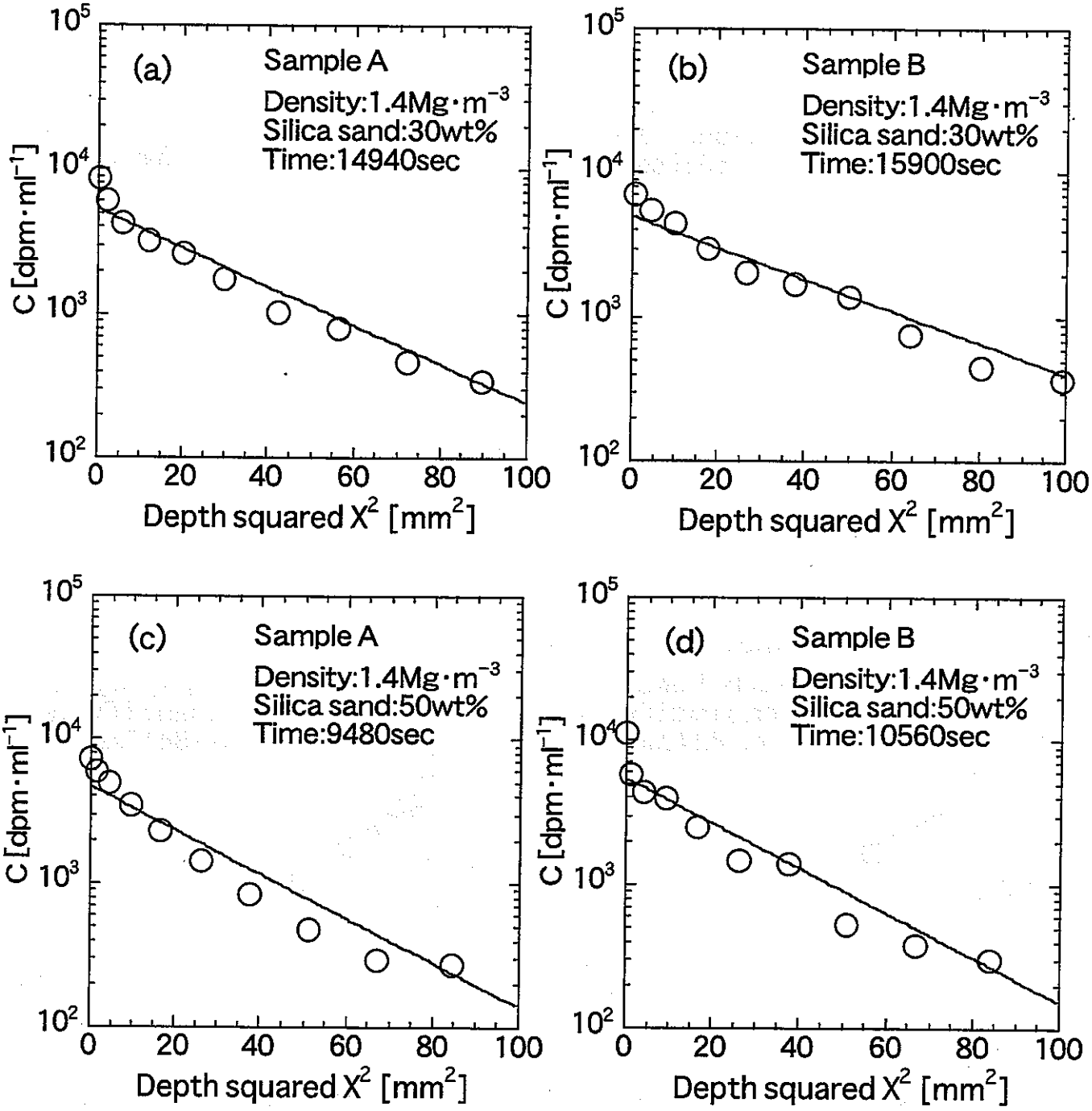

Correlations between the concentrations of HTO in bentonite and depth squared from the surface of the bentonite where tracer was pipetted for a dry density of 1.4 Mg•m^{-3}

(a) and (b); composition of silica sand in the bentonite, 30 wt%

(c) and (d); composition of silica sand in the bentonite, 50 wt%

Appendix II-c

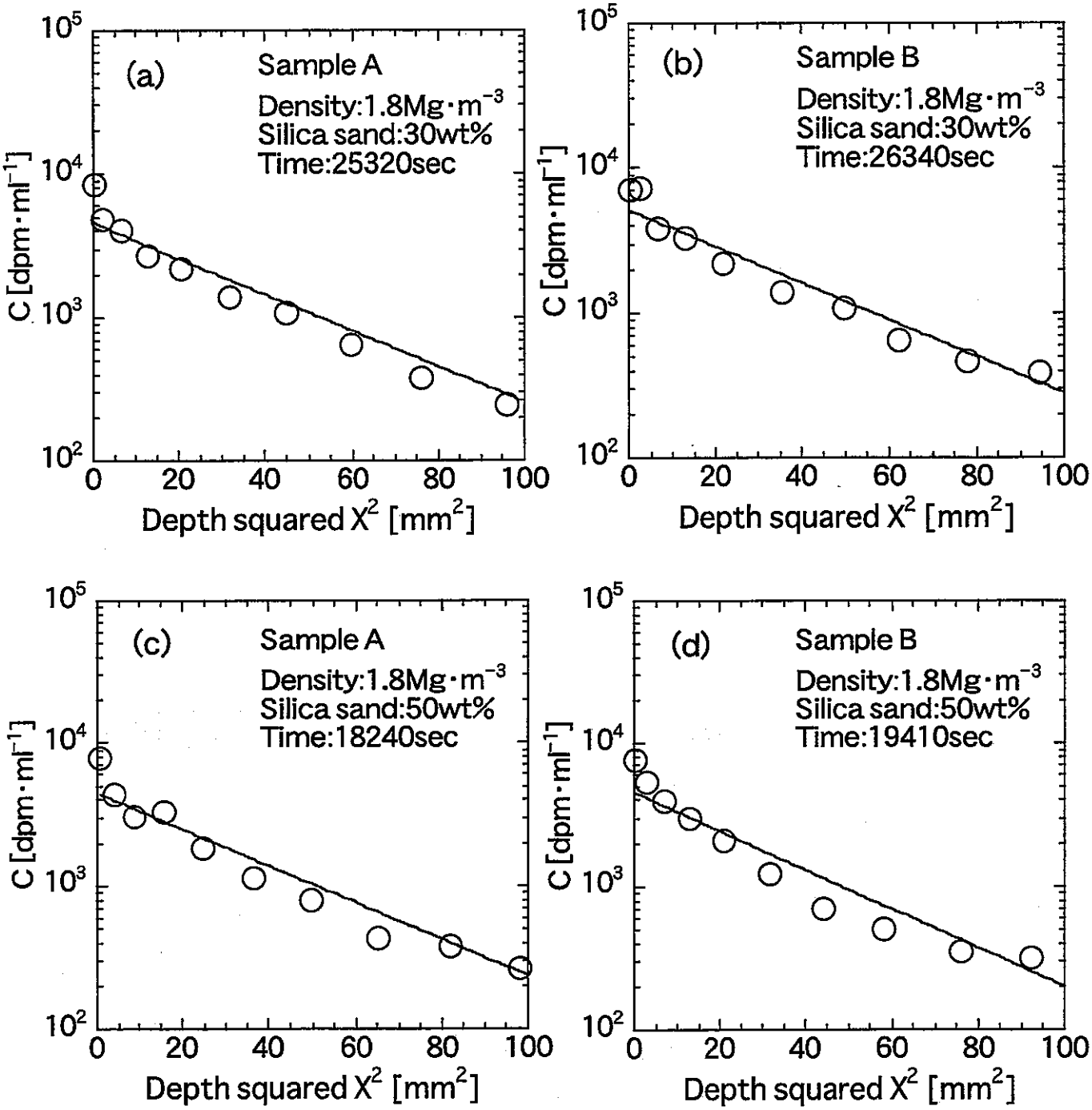

Correlations between the concentrations of HTO in bentonite and depth squared from the surface of the bentonite where tracer was pipetted for a dry density of 1.8 Mg•m^{-3}

(a) and (b); composition of silica sand in the bentonite, 30 wt%

(c) and (d); composition of silica sand in the bentonite, 50 wt%

Appendix III

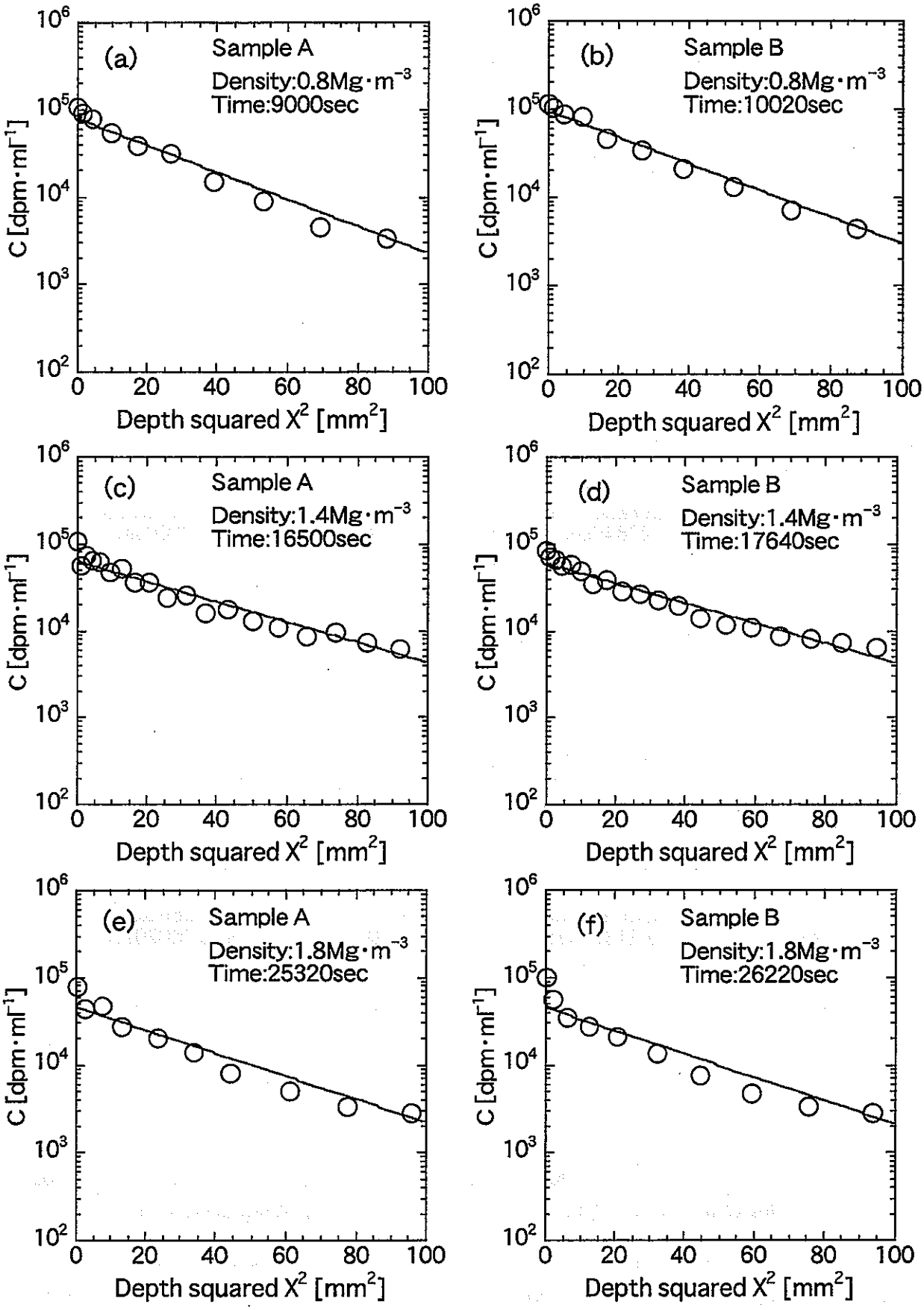

Correlations between the concentrations of HTO in bentonite and depth squared from the surface of the bentonite for the dry densities of 0.8, 1.4 and 1.8 Mg•m^{-3}

Appendix IV

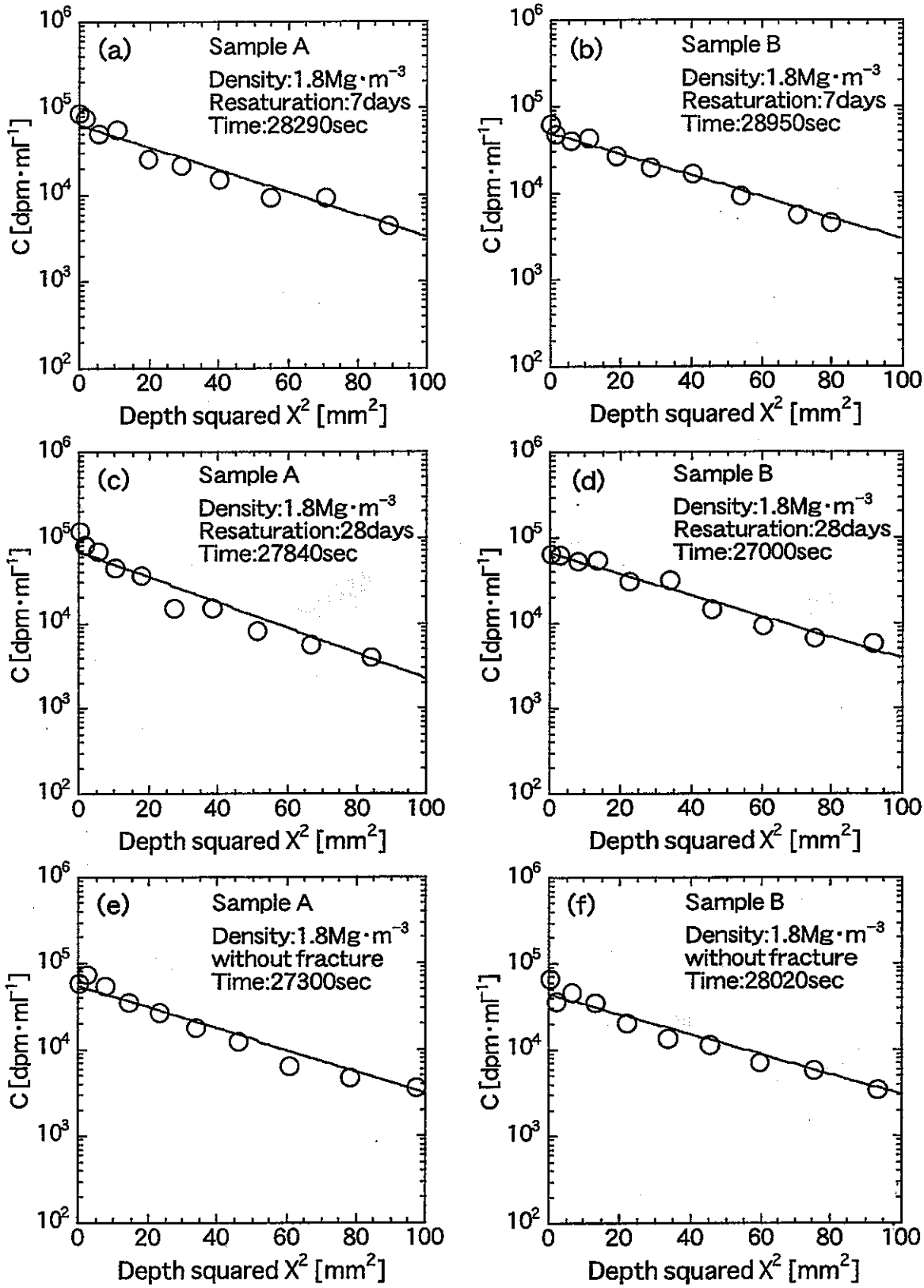

Correlations between the concentrations of HTO in bentonite and distance squared from the surface of the bentonite for the dry densities of 0.8, 1.4 and 1.8 Mg•m^{-3}

(a)~(d): bentonite with fracture, (e) and (f): bentonite without fracture